

# Let 2D Diffusion Model Know 3D-Consistency for Robust Text-to-3D Generation

Junyoung Seo<sup>\*1</sup> Wooseok Jang<sup>\*1</sup> Min-Seop Kwak<sup>\*1</sup> Jaehoon Ko<sup>1</sup> Hyeonsu Kim<sup>1</sup>  
 Junho Kim<sup>2</sup> Jin-Hwa Kim<sup>†2</sup> Jiyoung Lee<sup>†2</sup> Seungryong Kim<sup>†1</sup>

<sup>1</sup>Korea University <sup>2</sup>NAVER AI Lab

## Abstract

Text-to-3D generation has shown rapid progress in recent days with the advent of score distillation, a methodology of using pretrained text-to-2D diffusion models to optimize neural radiance field (NeRF) in the zero-shot setting. However, the lack of 3D awareness in the 2D diffusion models destabilizes score distillation-based methods from reconstructing a plausible 3D scene. To address this issue, we propose 3DFuse, a novel framework that incorporates 3D awareness into pretrained 2D diffusion models, enhancing the robustness and 3D consistency of score distillation-based methods. We realize this by first constructing a coarse 3D structure of a given text prompt and then utilizing projected, view-specific depth map as a condition for the diffusion model. Additionally, we introduce a training strategy that enables the 2D diffusion model learns to handle the errors and sparsity within the coarse 3D structure for robust generation, as well as a method for ensuring semantic consistency throughout all viewpoints of the scene. Our framework surpasses the limitations of prior arts, and has significant implications for 3D consistent generation of 2D diffusion models. Project page is available at <https://ku-cvlab.github.io/3DFuse/>.

## 1. Introduction

Text-to-3D generation, the task of generating realistic 3D models from texts [49, 26, 15], has rapidly grown in recent years to become an essential problem in computer vision and graphics. Recent approaches [38, 59, 25, 36] incorporate generative models with neural radiance field (NeRF) [32] to recover more plausible 3D scenes. Recent works along this line, such as DreamFusion [38] and Score Jacobian Chaining (SJC) [59], utilize large-scale diffusion models [45, 48] as a prior for optimizing NeRF. This methodology, named score distillation [38], enables suc-

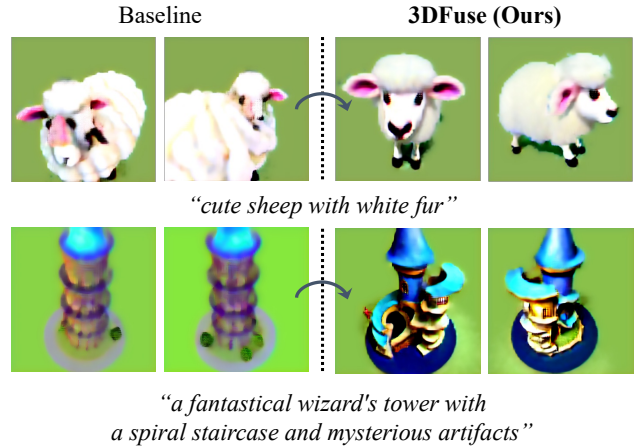


Figure 1: **Teaser.** 3DFuse enables view-consistent 3D generation given text prompt, while baseline (SJC [59]) often fails to recover plausible 3D.

cessful generation of a realistic 3D scene from a given text prompt.

However, 3D scenes generated by score distillation [38] are often prone to suffer from distortions and artifacts and sensitive to text prompts and random seeds, as shown in “Baseline” results of “a photo of cute hippo” in Fig. 1. One such failure is a 3D-incoherence problem, in which the rendered 3D scenes produce geometric features that belong to the frontal view (such as a face) multiple times at various viewpoints, as described in (a) of Fig. 2. This failure occurs due to the 2D diffusion model’s lack of awareness regarding 3D information, especially the camera pose. Since the diffusion model does not know from which direction the object is viewed, it is easily biased to produce frontal geometric features at all viewpoints, including side and back views, resulting in heavy distortions to the 3D scene.

An ideal solution to address this issue would be using a 3D aware diffusion model that can generate 3D-consistent images for any given scene viewpoint. However, naively training such a model from scratch would require extensive 3D data, whose size is minuscule compared to vast amounts

<sup>\*</sup>Equal contribution.

<sup>†</sup>Co-corresponding author.

of 2D data [51]. In addition, this approach cannot benefit from the powerful generalization capabilities of diffusion models trained on large 2D data. In light of this, a practical solution would be a middle-ground approach that combines the best of both worlds - a pretrained 2D diffusion model imbued with 3D awareness suitable for 3D-consistent NeRF optimization.

In this paper, we propose a novel framework, named 3DFuse, that effectively injects 3D awareness into pretrained 2D diffusion models. Given a text prompt, we first sample semantic code to fasten the semantic identity of the generated scene. The semantic code consists of a generated 2D image and a prompt embedding optimized from the pretrained diffusion model. Our consistency injection module takes this semantic code and obtains a viewpoint-specific depth map: a coarse 3D geometry constructed by an off-the-shelf model [35, 41, 61] from the generated image is projected to given viewpoint to build the depth map. The module then leverages the coarse depth map and the semantic code to inject 3D information into the diffusion model. As the predicted 3D geometry is bound to have errors, our module is able to handle the errors and coarseness within the depth maps. To this end, we introduce a sparse depth injector to implicitly correct erroneous depth information and LoRA [14] adaptation to preserve the semantics consistently. Our framework achieves significant improvement over previous works in generation quality and geometric consistency.

We summarize our contributions as follows:

- We propose a novel framework, called 3DFuse, that infuses 3D awareness into a pretrained 2D diffusion model, preserving the original generalization capability.
- By distilling the score of the diffusion model that produces 3D-consistent image, 3DFuse stably optimizes NeRF for view-consistent text-to-3D generation.
- We demonstrate the effectiveness of our framework qualitatively, and introduce a new metric for quantitative evaluation of 3D-consistency.

## 2. Related work

**Diffusion models.** Diffusion models [11, 54, 55] have gained much attention as generative models due to their stability, diversity, and scalability. Given these advantages, diffusion models have been applied in various fields, such as image translation [45, 56, 53], image editing [29, 19], and conditional generation [18, 45, 67]. Especially, text-to-image generation has been highlighted with the introduction of various guidance techniques [12, 2, 13]. GLIDE [34] utilizes CLIP [39] guidance to enable text-to-image generation, followed by large-scale text-to-image diffusion models such as Imagen [48], DALL-E2 [40], and Stable Dif-

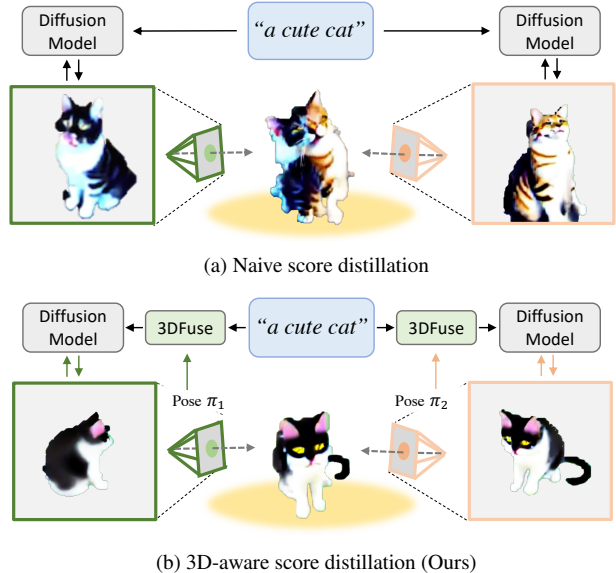


Figure 2: **Motivation.** (a) Previous methods [38, 55] only use noisy rendered images and prompt itself for score distillation through diffusion model, resulting in poor 3D coherence. (b) Our 3DFuse addresses this issue and shows robust performance in recovering 3D-consistent scene.

fusion [45]. The emergence of such models has led to the widespread utilization of pretrained text-to-image models for the tasks such as endowing additional conditions [60, 67] or performing manipulations [6, 23, 46].

**3D shape synthesis.** 3D shape synthesis is a task of constructing a 3D representation (*e.g.*, voxel grid [58, 24], mesh [8, 33, 10, 9, 7], point cloud [27, 69, 66], implicit fields [63, 28, 68, 62, 1]) from a given input, usually a single image. Early approaches such as PrGAN [5] and PointFlow [65] reconstruct single images into voxel and point cloud, while some works address specific tasks such as human mesh reconstruction [21, 17, 20, 16]. Recent works [35, 61] employ large generative models trained on large-scale data to achieve breakthroughs in 3D shape generation: Point-E [35] directly trains a diffusion model on point cloud data for a conditional point cloud generation. Another work, MCC [61], trains a masked autoencoding architecture on a large-scale 3D dataset Co3D [43] for point cloud construction from single images.

**Text-to-3D generation.** Existing text-to-3D generation methods generally employ pretrained vision-and-language models, such as CLIP [39] to generate 3D shapes and scenes from text prompts. DreamFields [15] incorporates CLIP with neural radiance fields (NeRF) [32] demonstrating the potential for zero-shot NeRF optimization using only CLIP as guidance. Recently, Dreamfusion [38] and SJC [59] have

demonstrated an impressive ability to generate NeRF with frozen diffusion models instead of CLIP. Among its follow-up works, Latent-NeRF [31] and Dream3D [64] are concurrent works and the most comparable to our work because they both utilize explicit 3D shapes to provide additional training signals in NeRF optimization. Dream3D directly initializes NeRF using generated SDF [37], while Latent-NeRF utilizes a user-provided mesh to give NeRF direct occupancy loss [30] for geometry optimization. Our approach differs from theirs in that we leverage the 3D priors to implicitly imbue the diffusion model itself with 3D awareness for consistent and robust NeRF generation, while they apply 3D priors directly to facilitate NeRF optimization.

### 3. Preliminaries

**Diffusion models.** Diffusion models are generative models that learn data distribution from a Gaussian distribution by a gradual denoising process [11]. Diffusion models define a deterministic forward process  $q(\cdot)$  that adds noise such that  $q(x_t|x_0) := \mathcal{N}(x_t; \alpha_t x_0, \sigma_t^2 I)$ , where  $x_t$  is a noised sample with noise level  $t$  and  $x_0$  is a clean sample, *e.g.*, original image, and  $\alpha_t$  and  $\sigma_t$  are pre-defined variables that control a noise schedule. The reverse process consists of denoising steps that progressively remove noise by modeling a neural network  $\mu_\theta(x_t, t)$  with parameters  $\theta$  that predicts  $x_0$  given  $x_t$ , and sampling from a posterior function derived from the forward process such that  $p_\theta(x_{t-1}|x_t) := q(x_{t-1}|x_t, x_0 = \mu_\theta(x_t, t))$ . As shown in DDPMs [11], noise approximation model  $\epsilon_\theta(x_t, t)$  can be used instead of  $\mu_\theta(x_t, t)$  as follows:

$$\epsilon_\theta(x_t, t) = \frac{x_t - \alpha_t \mu_\theta(x_t, t)}{\sigma_t}. \quad (1)$$

For a conditional generation, for instance, text-to-image diffusion models such as Stable Diffusion [45] receive a text prompt as an additional condition. Specifically, when a text prompt  $c$  is given, a mapping model  $T(\cdot)$  maps the prompt  $c$  into the embedding  $e = T(c)$ . Then, the embedding  $e$  is injected into the diffusion model. Formally, we denote the text-to-image diffusion model as  $\epsilon_\theta(x_t, t, T(c))$ . For the sake of brevity, we shall omit the variable  $t$  and refer to the function  $\epsilon_\theta(x_t, T(c))$ . In this case, the loss function for training the diffusion model is defined as follows:

$$\mathcal{L}_{\text{diff}}(\theta, x) = \mathbb{E}_{t, \epsilon} \left[ w(t) \|\epsilon_\theta(x_t, T(c)) - \epsilon\|_2^2 \right], \quad (2)$$

where  $\epsilon$  is a Gaussian noise and  $w(t)$  is a weighting function. Intuitively, this loss trains the model to predict the added Gaussian noise in the data.

**Score distillation to NeRF.** Optimizing NeRF with score distillation was first proposed in DreamFusion [38], which

optimizes NeRF parameters to follow the direction of the score predicted by the diffusion model, *i.e.*, the direction of higher-density regions [38]. Concurrent works such as SJC [59] and subsequent studies [25, 31] have been proposed based on similar intuition.

Specifically, let us denote  $\Theta$  as parameters of NeRF, and  $\mathcal{R}_\Theta(\pi)$  as a rendering function given a camera pose  $\pi$ . In DreamFusion and SJC, random camera pose  $\pi$  is sampled, and the diffusion model is utilized to infer the 2D score of the rendered image, *i.e.*,  $x = \mathcal{R}_\Theta(\pi)$ . This score is used to optimize the NeRF parameters  $\Theta$  by letting the rendered image move to the higher-density regions, *i.e.*, to be realistic. This can be explained as minimizing the loss function introduced in Eq. 2 with respect to the NeRF parameters  $\Theta$  instead of the diffusion model’s parameters  $\theta$  such that

$$\Theta^* = \underset{\Theta}{\operatorname{argmin}} \mathbb{E}_\pi \left[ \mathcal{L}_{\text{diff}}(\theta, x = \mathcal{R}_\Theta(\pi)) \right]. \quad (3)$$

In addition, the Jacobian term of the diffusion U-net  $\partial_{\epsilon_\theta}(x_t, T(c))/\partial x_t$  from the gradient of the loss function  $\nabla_\Theta \mathcal{L}_{\text{diff}}$  can be omitted for efficiency, and the new gradient can be formulated such that

$$\begin{aligned} \nabla_\Theta \mathcal{L}_{\text{SDS}}(\theta, x = \mathcal{R}_\Theta(\pi)) \\ \triangleq \mathbb{E}_{t, \epsilon} \left[ \tilde{w}(t) (\epsilon_\theta(x_t, T(c)) - \epsilon) \frac{\partial x}{\partial \Theta} \right], \end{aligned} \quad (4)$$

where  $\nabla_\Theta \mathcal{L}_{\text{SDS}}$  is a gradient of  $\mathcal{L}_{\text{diff}}$  with the U-net Jacobian term omitted, and  $\tilde{w}(t)$  is a weighting function.

## 4. Method

### 4.1. Motivation and overview

The score distillation-based text-to-3D methods [38, 25, 59] assume that maximizing the likelihood of images rendered from arbitrary viewpoints of a NeRF can be translated as maximizing the likelihood of the overall NeRF. Although this is a reasonable assumption, 2D diffusion models lack 3D awareness, which leads to inconsistent and distorted geometry of generated NeRF. To overcome this challenge and ensure NeRF’s 3D-consistency, we incorporate 3D awareness into the diffusion model.

Previous works [38, 59] attempt this by using the text prompts that roughly describe the camera viewpoint (*e.g.*, “side view”). However, this ad-hoc approach is severely limited: the ambiguity caused by the same text prompt representing a wide range of different pose values leaves NeRF generation vulnerable to geometric inconsistencies. A diffusion model directly conditioned on camera pose value  $\pi$  would be an ideal solution; however, this is not feasible due to the ambiguity in defining a canonical space for each 3D scene, and the difficulty of acquiring camera pose data.

To overcome these limitations, we present 3DFuse, our novel framework for effectively incorporating 3D awareness into pretrained text-to-image diffusion models [11, 45].

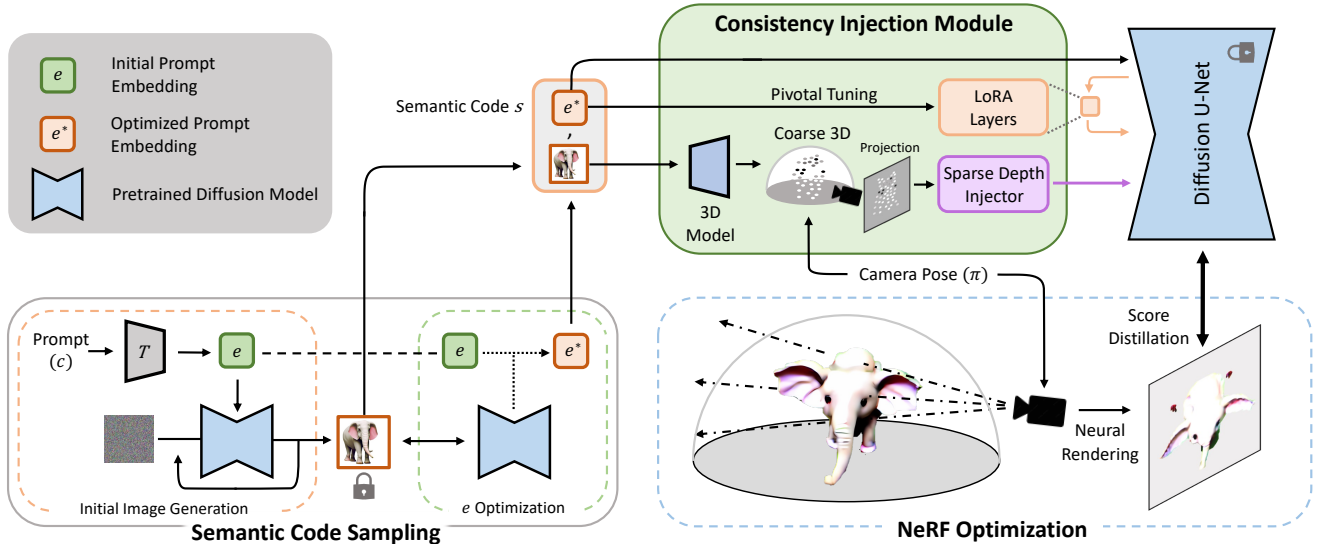


Figure 3: **Overall architecture of 3DFuse.** In the framework, semantic code is sampled to reduce the text prompt ambiguity by generating an image based on the text prompt and then optimizing the prompt’s embedding to match the generated image. Our consistency injection module receives this semantic code to synthesize view-specific depth maps as a condition to the diffusion U-net. The module also consists of a sparse depth injector to implicitly incorporate 3D awareness by utilizing an external 3D prior, and LoRA [14] layers to maintain semantic consistency.

Instead of having the diffusion model explicitly model camera pose  $\pi$ , our method constructs a coarse point cloud of an initially generated image  $\hat{x}$  through an off-the-shelf model [35, 61] and gives its viewpoint-specific depth map as a condition for the diffusion model. As the sparse depth map contains rich 3D information describing the scene from a given viewpoint, this approach effectively enables the diffusion model to generate NeRF in a 3D aware manner. In addition, to ensure the semantic similarity of NeRF across viewpoints, we introduce semantic code sampling, which constrains the entire 3D scene to a single semantic identity.

In the following, we describe our proposed methodology in detail. Our overall architecture is described in Fig. 3.

## 4.2. Semantic code sampling

The task of text-to-3D generation comes with a problem of inherent ambiguity within the text prompt. For instance, the text prompt “a cute cat” has color ambiguity, as it could refer to either a black or white cat. This ambiguity leads to the freedom to generate any image within this range, which harms the quality and coherence of the generated NeRF. Each score distillation step may guide NeRF toward widely different textures and semantics, which could result in a lack of coherence in the generated output. In Sec. 5.5, we provide a detailed demonstration of this phenomenon.

We introduce a simple yet effective technique to counter this text prompt ambiguity, which we call semantic code sampling. To specify the semantic identity of the scene we

optimize and thus reduce ambiguity, we first generate a 2D image  $\hat{x}$  from the text prompt  $c$ . Then, we optimize the text prompt embedding  $e$  to better fit the generated image, similarly to the textual inversion [6]:

$$e^* = \operatorname{argmin}_e \|\epsilon_\theta(\hat{x}_t, e) - \epsilon\|_2^2, \quad (5)$$

where  $\hat{x}_t$  is a noised image of the generated image  $\hat{x}$  with the noise  $\epsilon$  and the noise level  $t$ .

We refer to the pair of the generated image  $\hat{x}$  and the optimized embedding  $e^*$  as semantic code  $s$ , i.e.,  $s := (\hat{x}, e^*)$ , which are the inputs for our consistency injection module.

## 4.3. Incorporating a coarse 3D prior

Our approach aims to incorporate 3D awareness into pre-trained 2D diffusion models, and to achieve this we construct a coarse 3D representation of a given initial image and project it to a target viewpoint to make a sparse depth map. This sparse depth map is leveraged in our consistency injection module as a condition for 3D awareness.

Specifically, an off-the-shelf model  $D(\cdot)$  receives an image as input and outputs a coarse 3D representation, which is a sparse 3D point cloud in our architecture. We can choose  $D(\cdot)$  from a wide variety of models: it could be a point cloud generative model such as Point-E [35] or a single-image reconstruction model such as MCC [61]. Using them as 3D priors, we construct a sparse point cloud and project it to get a sparse depth map  $P$  corresponding to the



camera pose  $\pi$ :

$$P = \mathcal{P}(D(\hat{x}), \pi), \quad (6)$$

where  $\mathcal{P}(\cdot)$  is a depth-projection function. Subsequently, adopting the architecture of ControlNet [67], our sparse depth injector  $E_\phi$  receives the sparse depth map  $P$ , and its output features are added to the intermediate features within diffusion U-net of  $\epsilon_\theta(\hat{x}_t, e^*)$ , which can be further formulated such that  $\epsilon_\theta(\hat{x}_t, e^*; E_\phi(P))$ .

This approach brings significant advantages to score distillation-based NeRF generation. Unlike previous methods that directly optimize NeRF using only global text prompts, our  $3D_{Fuse}$  conditions the 3D optimization explicitly on the semantic code and its view-specific depth map. Not only does this enhance the 3D-consistency and fidelity of NeRF as intended, but it also encourages the 3D scene to be faithful to the semantic code, ensuring both geometric and semantic robustness of the generated 3D scene.

#### 4.4. Training the sparse depth injector

The point cloud obtained by the off-the-shelf 3D model inevitably contains errors and artifacts. It naturally causes its depth map to also have artifacts, as shown in Fig. 4(a). Therefore, our module must be able to handle both sparse geometry and the errors of the projected depth map.

To this end, we employ two training strategies for our sparse depth injector  $E_\phi(\cdot)$ . First, we train our injector using sparse depth maps, acquired by projecting point clouds from a point cloud dataset [43] to known viewpoints. By training our module with sparse depth map–image pairs, our model learns to interpolate and infer dense structural information from sparse depth. We impose strong augmentations on the point cloud data by randomly subsampling from it and adding randomly generated noisy points, which increases the robustness of our model against errors and noises present in the predicted sparse depth map. The texts for the corresponding images are obtained using the image caption model [4, 22].

Second, the injector  $E_\phi(\cdot)$  is also trained on predicted dense depth maps of text-to-image pairs, acquired using MiDaS [42]. This strengthens of model’s generalization capability, enabling it to infer structural information from categories that were not included in the 3D point cloud dataset for sparse depth training.

Combining the two, given the depth map  $P$  along with the corresponding image  $y$  and caption  $c$ , the training objective of the depth injector  $E_\phi$  is as follows:

$$\mathcal{L}_{\text{inject}}(\phi) = \mathbb{E}_{y,c,P,t,\epsilon} \left[ \|\epsilon_\theta(y_t, c; E_\phi(P)) - \epsilon\|_2^2 \right], \quad (7)$$

which is similar to Eq. 2, but only tunes the depth injector  $E_\phi$  while the diffusion model remains frozen. These training strategies enable our model to receive sparse and noisy

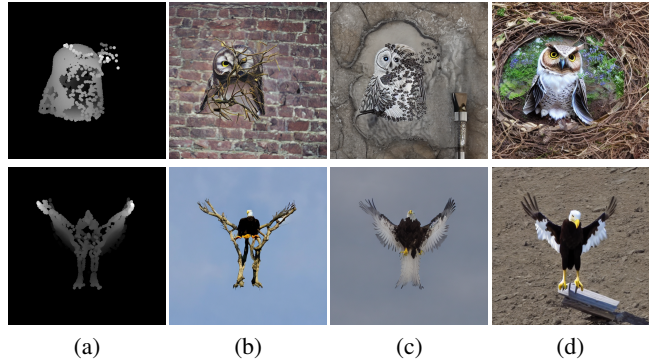


Figure 4: **Qualitative results conditioned on the sparse depth map.** Given sparse depth maps in (a), (b) are the results of depth-conditional Stable Diffusion, (c) are the results of ControlNet [67] trained on MiDaS [42] depths only, and (d) are our  $3D_{Fuse}$  results. The given text prompts are “a front view of an owl” and “a majestic eagle”.

depth maps directly as input and successfully infer dense and robust structural information from them, without needing any auxiliary depth completion network. Fig. 4 illustrates the effectiveness of our approach: our approach successfully generates realistic results without being restricted to the domain of the point cloud dataset. Note that the owl and eagle used in the illustration of Fig. 4 are not included in the category of the point cloud dataset [43] we use.

#### 4.5. Pivotal tuning for semantic consistency

To accomplish our objective, the diffusion model should produce a score that generates identical objects as much as possible from different camera poses, based on a semantic code. Although optimized embedding  $e^*$  preserves the semantics, we further enhance this by adopting LoRA [14] technique motivated by [47]. LoRA layers  $\psi$  consist of linear layers, inserted into the residual path of the attention layers in the diffusion U-net. Specifically, at test time, given an image  $\hat{x}$  generated from text prompt  $c$ , we fix the optimized embedding  $e^*$  and tune the LoRA layers  $\psi$  [44]:

$$\mathcal{L}_{\text{LoRA}}(\psi) = \mathbb{E}_{\epsilon,t} \left[ \|\epsilon_\theta(\hat{x}_t, e^*; \psi) - \epsilon\|_2^2 \right]. \quad (8)$$

Note that we only train the LoRA layers instead of the entire diffusion model to avoid overfitting to a specific viewpoint.

## 5. Experiments

### 5.1. Implementation details

We conduct all experiments with the Stable Diffusion [45] based on LDM [45], and train the sparse depth injector using a subset of the Co3D dataset [43] from the weights [67] trained image-text pairs along with depth maps predicted by MiDaS [42]. We conduct experiments with two off-the-shelf modules, mainly using Point-E [35] and in



Figure 5: **Qualitative comparisons for text-to-3D generation.** We compare our approach with Stable-DreamFusion [38, 57] and SJC [59]. Notice that all the results are rendered with a fixed random seed for a fair comparison. The geometric consistency of our approach can also be found at the **video results** provided in the project page.

Table 1: **User study.** The user study is conducted by surveying 102 participants to evaluate 3D coherence, prompt adherence, and rendering quality.

Method	3D coherence	Prompt adherence	Overall quality
3DFuse (Ours)	<b>60.1%</b>	<b>59.2%</b>	<b>60.9%</b>
Stable-DreamFusion [38, 57]	23.4%	23.4%	22.7%
SJC [59]	16.5%	17.4%	16.4%

Table 2: **Quantitative evaluation.** We compare 3D consistency with our proposed metric based on COLMAP [50].

Method	Variance ↓
3DFuse (Ours)	<b>0.0499</b>
SJC [59]	0.0870

certain experiments also leveraging MCC [61] with MiDaS. The details of score distillation and neural radiance field representation follow the settings of SJC [59], our baseline. In semantic code sampling, we adopt Karlo [3] based on unCLIP [40] because we find that it tends to follow user prompt more closely.

## 5.2. Text-to-3D generation

We compare 3DFuse to previous score distillation text-to-3D frameworks, DreamFusion [38] and Score Jacobian Chaining (SJC) [59]. All experiments including 3DFuse use Stable Diffusion [45] as a backbone, which is a publicly available large-scale text-to-image diffusion model. Because DreamFusion [38]’s official implementation uses publicly unavailable Imagen [48] model as its baseline, we instead resort to using Stable Diffusion [45] for implementation, which we call Stable-DreamFusion [57].

**Qualitative evaluation.** We present our qualitative evaluation in Fig. 5, which demonstrates that the neural radiance fields generated by our framework surpass previous methods in both fidelity and geometric consistency. While previous methods produce inconsistent, distorted geometry in multiple regions, our method generates robust geometry at every viewpoint, as evidenced by the figure as well as video results provided in the project page. Furthermore, we present the qualitative results of our approach when utilizing MCC [61] for the 3D prior in Fig. 6, which shows generating high-quality 3D content as well.

**Quantitative evaluation.** It is difficult to conduct a quantitative evaluation on a zero-shot text-to-3D generative model due to the absence of ground truth 3D scenes corresponding to the text prompts. Existing works provide additional user studies [25] or employ CLIP R-Precision [15,



“a toy bicycle” “a toy plane” “a backpack” “a penguin”

Figure 6: **Qualitative results of 3DFuse with MCC [61].** Our 3DFuse framework yields high-fidelity rendering results even with MCC [61].

38]. However, CLIP R-Precision only measures retrieval accuracy through projected 2D image and text input, so it is not suitable for quantifying the geometric consistency of a 3D scene.

Instead, we propose a new metric that utilizes COLMAP [50] to measure the consistency of a generated 3D scene. We based on the fact that the accuracy of COLMAP camera pose optimization is dependent upon the robustness and consistency of 3D surfaces, as stated in [52]. We sample 100 uniformly spaced camera poses from a hemisphere of fixed radius, at identical elevation, all directed towards the sphere’s center, and render 100 images of the 3D scene. COLMAP predicts the camera pose of each image for reconstruction. We then measure the difference between the predicted camera poses of two adjacent images at the rendering stage. The variance of these values is used as our metric for 3D-consistency evaluation. High variance indicates inaccuracy in the predicted camera poses, which corresponds to 3D inconsistency that makes optimization for COLMAP difficult. Additional details of our metric are provided in the supplementary materials.

Using this metric, we compare the consistency of scenes generated by our 3DFuse and SJC. In Table 2, we report the average of variance scores over 42 generated 3D scenes. Our 3DFuse framework outperforms SJC by a large margin, quantitatively demonstrating that our framework achieves more geometrically consistent text-to-3D generation.

**User study.** We have conducted a user study with 102 participants, which is shown in Table. 1. We have asked the participants to choose their preferred result in terms of 3D coherence, prompt adherence, and overall quality between Stable-DreamFusion [38, 57], SJC [59], and our 3DFuse. The results show that 3DFuse generates 3D scenes that the majority of people judge as having higher fidelity and better geometric consistency than previous methods. Further details are described in the supplementary material.



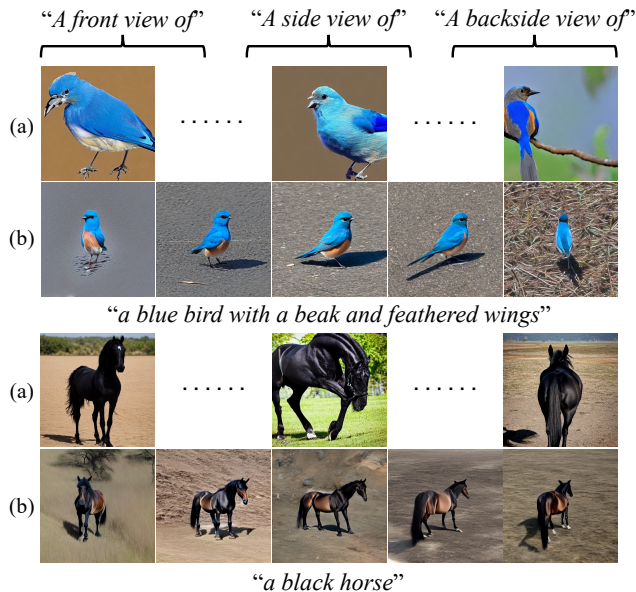


Figure 7: **Qualitative comparison of view-dependent image generation results.** (a) Results of view augmented prompting, and (b) our results with 3DFuse framework.

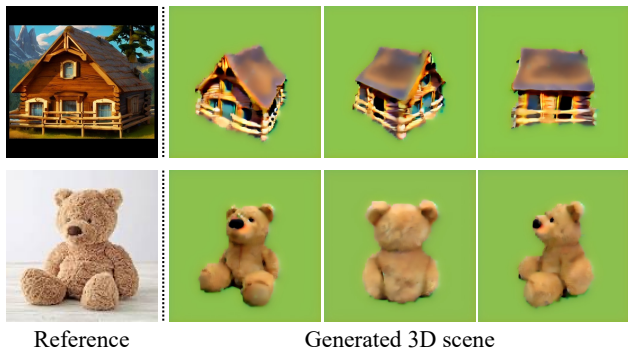


Figure 8: **Qualitative result for image-conditional 3D generation.** When a reference image is directly given as input, 3DFuse successfully captures the image’s style and appearance for coherent 3D scene generation.

### 5.3. View-dependent text-to-image generation

We conduct text-to-image generation experiments with 3DFuse to verify our framework’s capability to infuse 3D awareness into 2D diffusion models. We observe whether the images are generated in a 3D aware manner when view-points are given as conditions through our 3DFuse framework. Fig. 7 well demonstrates the effectiveness of our framework: it allows for highly precise control of the camera pose in 2D images, with even small changes in view-point being reflected well on the generated images. Our approach shows superior performance to previous prompt-based methods (*e.g.* “A front view of”) regarding both precision and controllability of injected 3D awareness.

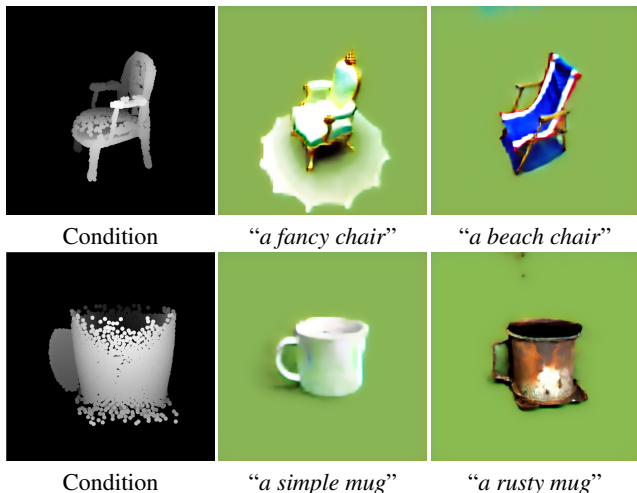


Figure 9: **3D reconstruction with different prompts given a single 3D structure.** The first column represents the given point clouds as conditions, and the second and third columns show synthesized results.

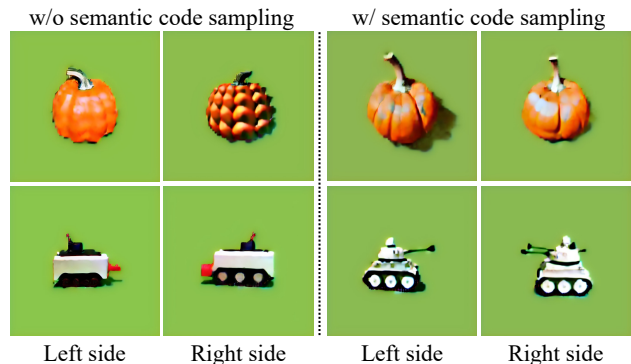


Figure 10: **Ablation study on semantic code sampling.** The given prompts are “a round orange pumpkin with a stem and a textured surface” (top) and “a product photo of a toy tank” (bottom).

### 5.4. Image-conditional 3D generation

In this experiment, instead of generating the initial image from a text prompt, we directly give an input image as the initial image  $\hat{x}$  of our semantic code, which effectively re-configures our framework as an image-conditional setting. Fig. 8 displays impressive results: it shows that our architecture successfully captures the overall structure and appearance of the input image for NeRF generation. This has interesting implications, as it demonstrates that our framework has a certain degree of 3D reconstruction capability.

### 5.5. Analysis and ablation study

**Different prompts with single 3D representation.** 3D representation, *i.e.*, point cloud obtained from off-the-shelf models [35, 61] is typically coarse and sparse. To investi-



Figure 11: **Qualitative comparison for robustness.** When given a single prompt, 3DFuse demonstrates robust performance even in random seed variations. We visualize the outputs generated from the fixed seed from 0 to 4.



gate how the diffusion model implicitly refines the coarse 3D structure, we conduct an ablation study using a fixed point cloud and different text prompts instead of inferring a point cloud from the initial image  $\hat{x}$  of semantic code  $s$ . Fig. 9 shows that our 3DFuse is flexible in responding to the error and sparsity inherent in the point cloud, robustly interpreting the depth map in accordance with the semantics of text input.

**Semantic code sampling.** We conduct an ablation study on semantic code sampling in our 3DFuse framework. The results in the first two columns of Fig. 10 show significant differences in geometry (pumpkin’s smooth left surface and bumpy right surface) and semantic details (the tank’s absence of wheel on the left) without semantic code sampling, depending on viewpoints. In contrast, using semantic code sampling ensures both geometric and semantic consistency across viewpoints, demonstrating its prominence in preserving the semantic identity of the 3D scene.

**Robustness.** We experiment with fixed prompts and changing random seeds to verify the robustness of our approach compared to previous works [38, 57, 59]. Fig. 11 demonstrates that our approach exhibits robust performance and is far less sensitive to random seeds compared to previous works.

## 6. Conclusion

In this paper, we address the 3D-incoherence problem in text-to-3D generation by score distillation. We propose a novel framework, dubbed 3DFuse, that effectively incorporates 3D awareness into a pretrained 2D diffusion model. Our method utilizes viewpoint-specific depth maps from a coarse 3D structure, complemented with a sparse depth injector and semantic code sampling for semantic consistency. Our approach offers a practical solution for addressing the limitations of current text-to-3D generation techniques and opens up possibilities for generating more realistic 3D scenes from text prompts. Our experimental results demonstrate the effectiveness of our framework, outperforming previous models in quantitative metric and qualitative human evaluation.

## References

[1] Zezhou Cheng, Menglei Chai, Jian Ren, Hsin-Ying Lee, Kyle Olszewski, Zeng Huang, Subhansu Maji, and Sergey Tulyakov. Cross-modal 3d shape generation and manipulation. In *Computer Vision—ECCV 2022: 17th European Conference, Tel Aviv, Israel, October 23–27, 2022, Proceedings, Part III*, pages 303–321. Springer, 2022.

[2] Prafulla Dhariwal and Alexander Nichol. Diffusion models beat gans on image synthesis. *NeurIPS*, 34:8780–8794, 2021.

[3] Jiseob Kim Donghoon Lee, Jongmin Kim Jisu Choi, Woonhyuk Baek Minwoo Byeon, and Saehoon Kim. Karlo-v1.0.alpha on coyo-100m and cc15m. <https://github.com/kakaobrain/karlo>, 2022.

[4] Alexey Dosovitskiy, Lucas Beyer, Alexander Kolesnikov, Dirk Weissenborn, Xiaohua Zhai, Thomas Unterthiner, Mostafa Dehghani, Matthias Minderer, Georg Heigold, Sylvain Gelly, et al. An image is worth 16x16 words: Transformers for image recognition at scale. In *ICLR*, 2020.

[5] Matheus Gadelha, Subhansu Maji, and Rui Wang. 3d shape induction from 2d views of multiple objects. In *2017 International Conference on 3D Vision (3DV)*, pages 402–411. IEEE, 2017.

[6] Rinon Gal, Yuval Alaluf, Yuval Atzmon, Or Patashnik, Amit H Bermano, Gal Chechik, and Daniel Cohen-Or. An image is worth one word: Personalizing text-to-image generation using textual inversion. *arXiv preprint arXiv:2208.01618*, 2022.

[7] Lin Gao, Tong Wu, Yu-Jie Yuan, Ming-Xian Lin, Yu-Kun Lai, and Hao Zhang. Tm-net: Deep generative networks for textured meshes. *ACM Transactions on Graphics (TOG)*, 40(6):263:1–263:15, 2021.

[8] Lin Gao, Jie Yang, Tong Wu, Yu-Jie Yuan, Hongbo Fu, Yu-Kun Lai, and Hao Zhang. Sdm-net: Deep generative network for structured deformable mesh. *ACM Transactions on Graphics (TOG)*, 38(6):1–15, 2019.

[9] Kunal Gupta. *Neural mesh flow: 3d manifold mesh generation via diffeomorphic flows*. University of California, San Diego, 2020.

[10] Paul Henderson, Vagia Tsiminaki, and Christoph H Lampert. Leveraging 2d data to learn textured 3d mesh generation. In *Proceedings of the IEEE/CVF Conference on Computer Vision and Pattern Recognition*, pages 7498–7507, 2020.

[11] Jonathan Ho, Ajay Jain, and Pieter Abbeel. Denoising diffusion probabilistic models. *Advances in Neural Information Processing Systems*, 33:6840–6851, 2020.

[12] Jonathan Ho and Tim Salimans. Classifier-free diffusion guidance. 2022.

[13] Susung Hong, Gyuseong Lee, Wooseok Jang, and Seungryong Kim. Improving sample quality of diffusion models using self-attention guidance. *arXiv preprint arXiv:2210.00939*, 2022.

[14] Edward J Hu, Yelong Shen, Phillip Wallis, Zeyuan Allen-Zhu, Yuanzhi Li, Shean Wang, Lu Wang, and Weizhu Chen. Lora: Low-rank adaptation of large language models. *arXiv preprint arXiv:2106.09685*, 2021.

[15] Ajay Jain, Ben Mildenhall, Jonathan T Barron, Pieter Abbeel, and Ben Poole. Zero-shot text-guided object generation with dream fields. In *Proceedings of the IEEE/CVF Conference on Computer Vision and Pattern Recognition*, pages 867–876, 2022.

[16] Hanbyul Joo, Natalia Neverova, and Andrea Vedaldi. Exemplar fine-tuning for 3d human model fitting towards in-the-wild 3d human pose estimation. In *2021 International Conference on 3D Vision (3DV)*, pages 42–52. IEEE, 2021.

[17] Angjoo Kanazawa, Michael J Black, David W Jacobs, and Jitendra Malik. End-to-end recovery of human shape and

- pose. In *Proceedings of the IEEE conference on computer vision and pattern recognition*, pages 7122–7131, 2018.
- [18] Yossi Kanizo, David Hay, and Isaac Keslassy. Palette: Distributing tables in software-defined networks. In *2013 Proceedings IEEE INFOCOM*, pages 545–549. IEEE, 2013.
- [19] Gwanghyun Kim, Taesung Kwon, and Jong Chul Ye. Diffusionclip: Text-guided diffusion models for robust image manipulation. In *Proceedings of the IEEE/CVF Conference on Computer Vision and Pattern Recognition*, pages 2426–2435, 2022.
- [20] Nikos Kolotouros, Georgios Pavlakos, Michael J Black, and Kostas Daniilidis. Learning to reconstruct 3d human pose and shape via model-fitting in the loop. In *Proceedings of the IEEE/CVF international conference on computer vision*, pages 2252–2261, 2019.
- [21] Nikos Kolotouros, Georgios Pavlakos, and Kostas Daniilidis. Convolutional mesh regression for single-image human shape reconstruction. In *Proceedings of the IEEE/CVF Conference on Computer Vision and Pattern Recognition*, pages 4501–4510, 2019.
- [22] Ankur Kumar. The illustrated image captioning using transformers. *ankur3107.github.io*, 2022.
- [23] Mingi Kwon, Jaeseok Jeong, and Youngjung Uh. Diffusion models already have a semantic latent space. *arXiv preprint arXiv:2210.10960*, 2022.
- [24] Jun Li, Kai Xu, Siddhartha Chaudhuri, Ersin Yumer, Hao Zhang, and Leonidas Guibas. Grass: Generative recursive autoencoders for shape structures. *ACM Transactions on Graphics (TOG)*, 36(4):1–14, 2017.
- [25] Chen-Hsuan Lin, Jun Gao, Luming Tang, Towaki Takikawa, Xiaohui Zeng, Xun Huang, Karsten Kreis, Sanja Fidler, Ming-Yu Liu, and Tsung-Yi Lin. Magic3d: High-resolution text-to-3d content creation. *arXiv preprint arXiv:2211.10440*, 2022.
- [26] Zhengzhe Liu, Peng Dai, Ruihui Li, Xiaojuan Qi, and Chi-Wing Fu. Iss: Image as stetting stone for text-guided 3d shape generation. *arXiv preprint arXiv:2209.04145*, 2022.
- [27] Andrew Luo, Tianqin Li, Wen-Hao Zhang, and Tai Sing Lee. Surfgen: Adversarial 3d shape synthesis with explicit surface discriminators. In *Proceedings of the IEEE/CVF International Conference on Computer Vision*, pages 16238–16248, 2021.
- [28] Andrew Luo, Tianqin Li, Wen-Hao Zhang, and Tai Sing Lee. Surfgen: Adversarial 3d shape synthesis with explicit surface discriminators. In *Proceedings of the IEEE/CVF International Conference on Computer Vision*, pages 16238–16248, 2021.
- [29] Chenlin Meng, Yutong He, Yang Song, Jiaming Song, Jiajun Wu, Jun-Yan Zhu, and Stefano Ermon. Sdedit: Guided image synthesis and editing with stochastic differential equations. In *International Conference on Learning Representations*, 2021.
- [30] Lars Mescheder, Michael Oechsle, Michael Niemeyer, Sebastian Nowozin, and Andreas Geiger. Occupancy networks: Learning 3d reconstruction in function space. In *Proceedings of the IEEE/CVF conference on computer vision and pattern recognition*, pages 4460–4470, 2019.
- [31] Gal Metzer, Elad Richardson, Or Patashnik, Raja Giryes, and Daniel Cohen-Or. Latent-nerf for shape-guided generation of 3d shapes and textures. *arXiv preprint arXiv:2211.07600*, 2022.
- [32] Ben Mildenhall, Pratul P Srinivasan, Matthew Tancik, Jonathan T Barron, Ravi Ramamoorthi, and Ren Ng. Nerf: Representing scenes as neural radiance fields for view synthesis. volume 65, pages 99–106. ACM New York, NY, USA, 2021.
- [33] Charlie Nash, Yaroslav Ganin, SM Ali Eslami, and Peter Battaglia. Polygen: An autoregressive generative model of 3d meshes. pages 7220–7229, 2020.
- [34] Alex Nichol, Prafulla Dhariwal, Aditya Ramesh, Pranav Shyam, Pamela Mishkin, Bob McGrew, Ilya Sutskever, and Mark Chen. Glide: Towards photorealistic image generation and editing with text-guided diffusion models. *arXiv preprint arXiv:2112.10741*, 2021.
- [35] Alex Nichol, Heewoo Jun, Prafulla Dhariwal, Pamela Mishkin, and Mark Chen. Point-e: A system for generating 3d point clouds from complex prompts. *arXiv preprint arXiv:2212.08751*, 2022.
- [36] Roy Or-El, Xuan Luo, Mengyi Shan, Eli Shechtman, Jeong Joon Park, and Ira Kemelmacher-Shlizerman. Stylesdf: High-resolution 3d-consistent image and geometry generation. In *Proceedings of the IEEE/CVF Conference on Computer Vision and Pattern Recognition*, pages 13503–13513, 2022.
- [37] Jeong Joon Park, Peter Florence, Julian Straub, Richard Newcombe, and Steven Lovegrove. DeepSDF: Learning continuous signed distance functions for shape representation. In *Proceedings of the IEEE/CVF conference on computer vision and pattern recognition*, pages 165–174, 2019.
- [38] Ben Poole, Ajay Jain, Jonathan T Barron, and Ben Mildenhall. Dreamfusion: Text-to-3d using 2d diffusion. *arXiv preprint arXiv:2209.14988*, 2022.
- [39] Alec Radford, Jong Wook Kim, Chris Hallacy, Aditya Ramesh, Gabriel Goh, Sandhini Agarwal, Girish Sastry, Amanda Askell, Pamela Mishkin, Jack Clark, et al. Learning transferable visual models from natural language supervision. In *International conference on machine learning*, pages 8748–8763. PMLR, 2021.
- [40] Aditya Ramesh, Prafulla Dhariwal, Alex Nichol, Casey Chu, and Mark Chen. Hierarchical text-conditional image generation with clip latents. *arXiv preprint arXiv:2204.06125*, 2022.
- [41] René Ranftl, Alexey Bochkovskiy, and Vladlen Koltun. Vision transformers for dense prediction. In *Proceedings of the IEEE/CVF International Conference on Computer Vision*, pages 12179–12188, 2021.
- [42] René Ranftl, Katrin Lasinger, David Hafner, Konrad Schindler, and Vladlen Koltun. Towards robust monocular depth estimation: Mixing datasets for zero-shot cross-dataset transfer. *IEEE transactions on pattern analysis and machine intelligence*, 44(3):1623–1637, 2020.
- [43] Jeremy Reizenstein, Roman Shapovalov, Philipp Henzler, Luca Sbordone, Patrick Labatut, and David Novotny. Common objects in 3d: Large-scale learning and evaluation of

- real-life 3d category reconstruction. In *Proceedings of the IEEE/CVF International Conference on Computer Vision*, pages 10901–10911, 2021.
- [44] Daniel Roich, Ron Mokady, Amit H Bermano, and Daniel Cohen-Or. Pivotal tuning for latent-based editing of real images. *ACM Transactions on Graphics (TOG)*, 42(1):1–13, 2022.
- [45] Robin Rombach, Andreas Blattmann, Dominik Lorenz, Patrick Esser, and Björn Ommer. High-resolution image synthesis with latent diffusion models. In *Proceedings of the IEEE/CVF Conference on Computer Vision and Pattern Recognition*, pages 10684–10695, 2022.
- [46] Nataniel Ruiz, Yuanzhen Li, Varun Jampani, Yael Pritch, Michael Rubinstein, and Kfir Aberman. Dreambooth: Fine tuning text-to-image diffusion models for subject-driven generation. *arXiv preprint arXiv:2208.12242*, 2022.
- [47] Simo Ryu. Low-rank adaptation for fast text-to-image diffusion fine-tuning. <https://github.com/cloneofsimo/lora>, 2022.
- [48] Chitwan Saharia, William Chan, Saurabh Saxena, Lala Li, Jay Whang, Emily Denton, Seyed Kamyar Seyed Ghasemipour, Burcu Karagol Ayan, S Sara Mahdavi, Rapha Gontijo Lopes, et al. Photorealistic text-to-image diffusion models with deep language understanding. *arXiv preprint arXiv:2205.11487*, 2022.
- [49] Aditya Sanghi, Hang Chu, Joseph G Lambourne, Ye Wang, Chin-Yi Cheng, Marco Fumero, and Kamal Rahimi Malekshah. Clip-forge: Towards zero-shot text-to-shape generation. In *Proceedings of the IEEE/CVF Conference on Computer Vision and Pattern Recognition*, pages 18603–18613, 2022.
- [50] Johannes L Schonberger and Jan-Michael Frahm. Structure-from-motion revisited. In *Proceedings of the IEEE conference on computer vision and pattern recognition*, pages 4104–4113, 2016.
- [51] Christoph Schuhmann, Romain Beaumont, Richard Vencu, Cade Gordon, Ross Wightman, Mehdi Cherti, Theo Coombes, Aarush Katta, Clayton Mullis, Mitchell Wortsman, et al. Laion-5b: An open large-scale dataset for training next generation image-text models. *arXiv preprint arXiv:2210.08402*, 2022.
- [52] Katja Schwarz, Yiyi Liao, Michael Niemeyer, and Andreas Geiger. Graf: Generative radiance fields for 3d-aware image synthesis. *Advances in Neural Information Processing Systems*, 33:20154–20166, 2020.
- [53] Junyoung Seo, Gyuseong Lee, Seokju Cho, Jiyoung Lee, and Seungryong Kim. Midms: Matching interleaved diffusion models for exemplar-based image translation. *arXiv preprint arXiv:2209.11047*, 2022.
- [54] Jiaming Song, Chenlin Meng, and Stefano Ermon. Denoising diffusion implicit models. 2020.
- [55] Yang Song, Jascha Sohl-Dickstein, Diederik P Kingma, Abhishek Kumar, Stefano Ermon, and Ben Poole. Score-based generative modeling through stochastic differential equations. 2020.
- [56] Xuan Su, Jiaming Song, Chenlin Meng, and Stefano Ermon. Dual diffusion implicit bridges for image-to-image translation. In *International Conference on Learning Representations*, 2022.
- [57] Jiayang Tang. Stable-dreamfusion: Text-to-3d with stable-diffusion, 2022. <https://github.com/ashawkey/stable-dreamfusion>.
- [58] Maxim Tatarchenko, Alexey Dosovitskiy, and Thomas Brox. Octree generating networks: Efficient convolutional architectures for high-resolution 3d outputs. In *Proceedings of the IEEE international conference on computer vision*, pages 2088–2096, 2017.
- [59] Haochen Wang, Xiaodan Du, Jiahao Li, Raymond A Yeh, and Greg Shakhnarovich. Score jacobian chaining: Lifting pretrained 2d diffusion models for 3d generation. *arXiv preprint arXiv:2212.00774*, 2022.
- [60] Tengfei Wang, Ting Zhang, Bo Zhang, Hao Ouyang, Dong Chen, Qifeng Chen, and Fang Wen. Pretraining is all you need for image-to-image translation. *arXiv preprint arXiv:2205.12952*, 2022.
- [61] Chao-Yuan Wu, Justin Johnson, Jitendra Malik, Christoph Feichtenhofer, and Georgia Gkioxari. Multiview compressive coding for 3D reconstruction. *arXiv preprint arXiv:2301.08247*, 2023.
- [62] Rundi Wu and Changxi Zheng. Learning to generate 3d shapes from a single example. *arXiv preprint arXiv:2208.02946*, 2022.
- [63] Rundi Wu, Yixin Zhuang, Kai Xu, Hao Zhang, and Baoquan Chen. Pq-net: A generative part seq2seq network for 3d shapes. In *Proceedings of the IEEE/CVF Conference on Computer Vision and Pattern Recognition*, pages 829–838, 2020.
- [64] Jiale Xu, Xintao Wang, Weihao Cheng, Yan-Pei Cao, Ying Shan, Xiaohu Qie, and Shenghua Gao. Dream3d: Zero-shot text-to-3d synthesis using 3d shape prior and text-to-image diffusion models. *arXiv preprint arXiv:2212.14704*, 2022.
- [65] Guandao Yang, Xun Huang, Zekun Hao, Ming-Yu Liu, Serge Belongie, and Bharath Hariharan. Pointflow: 3d point cloud generation with continuous normalizing flows. In *Proceedings of the IEEE/CVF international conference on computer vision*, pages 4541–4550, 2019.
- [66] Xiaohui Zeng, Arash Vahdat, Francis Williams, Zan Gojcic, Or Litany, Sanja Fidler, and Karsten Kreis. Lion: Latent point diffusion models for 3d shape generation. 2022.
- [67] Lvmin Zhang and Maneesh Agrawala. Adding conditional control to text-to-image diffusion models. *arXiv preprint arXiv:2302.05543*, 2023.
- [68] X Zheng, Yang Liu, P Wang, and Xin Tong. Sdf-stylegan: Implicit sdf-based stylegan for 3d shape generation. In *Computer Graphics Forum*, volume 41, pages 52–63. Wiley Online Library, 2022.
- [69] Linqi Zhou, Yilun Du, and Jiajun Wu. 3d shape generation and completion through point-voxel diffusion. In *Proceedings of the IEEE/CVF International Conference on Computer Vision*, pages 5826–5835, 2021.